



Measurements of branching fractions and direct CP -violating asymmetries in $B^+ \rightarrow K^+\pi^0$ and $\pi^+\pi^0$ decays using 2019 and 2020 Belle II data

- F. Abudinén,⁴⁹ I. Adachi,^{25,22} R. Adak,¹⁹ K. Adamczyk,⁷⁵ P. Ahlburg,¹¹⁰ J. K. Ahn,⁵⁷ H. Aihara,¹²⁸ N. Akopov,¹³⁴ A. Aloisio,^{99,42} F. Ameli,⁴⁶ L. Andricek,⁶⁶ N. Anh Ky,^{39,14} D. M. Asner,³ H. Atmacan,¹¹² V. Aulchenko,^{4,77} T. Aushev,²⁷ V. Aushev,⁹⁰ T. Aziz,⁹¹ V. Babu,¹² S. Bacher,⁷⁵ S. Baehr,⁵³ S. Bahinipati,²⁹ A. M. Bakich,¹²⁷ P. Bambade,¹⁰⁷ Sw. Banerjee,¹¹⁷ S. Bansal,⁸² M. Barrett,²⁵ G. Batignani,^{102,45} J. Baudot,¹⁰⁸ A. Beaulieu,¹³⁰ J. Becker,⁵³ P. K. Behera,³² M. Bender,⁶² J. V. Bennett,¹²¹ E. Bernieri,⁴⁷ F. U. Bernlochner,¹¹⁰ M. Bertemes,³⁵ E. Bertholet,⁹³ M. Bessner,¹¹⁴ S. Bettarini,^{102,45} V. Bhardwaj,²⁸ B. Bhuyan,³⁰ F. Bianchi,^{104,48} T. Bilka,⁷ S. Bilokhin,⁶² D. Biswas,¹¹⁷ A. Bobrov,^{4,77} A. Bondar,^{4,77} G. Bonvicini,¹³² A. Bozek,⁷⁵ M. Bračko,^{119,89} P. Branchini,⁴⁷ N. Braun,⁵³ R. A. Briere,⁵ T. E. Browder,¹¹⁴ D. N. Brown,¹¹⁷ A. Budano,⁴⁷ L. Burmistrov,¹⁰⁷ S. Bussino,^{103,47} M. Campajola,^{99,42} L. Cao,¹¹⁰ G. Caria,¹²⁰ G. Casarosa,^{102,45} C. Cecchi,^{101,44} D. Červenkov,⁷ M.-C. Chang,¹⁸ P. Chang,⁷³ R. Cheaib,¹² V. Chekelian,⁶⁵ C. Chen,⁵⁴ Y. Q. Chen,¹²⁴ Y.-T. Chen,⁷³ B. G. Cheon,²⁴ K. Chilikin,⁶⁰ K. Chirapatpimol,⁸ H.-E. Cho,²⁴ K. Cho,⁵⁶ S.-J. Cho,¹³⁵ S.-K. Choi,²³ S. Choudhury,³¹ D. Cinabro,¹³² L. Corona,^{102,45} L. M. Cremaldi,¹²¹ D. Cuesta,¹⁰⁸ S. Cunliffe,¹² T. Czank,¹²⁹ N. Dash,³² F. Dattola,¹² E. De La Cruz-Burelo,⁶ G. de Marino,¹⁰⁷ G. De Nardo,^{99,42} M. De Nuccio,¹² G. De Pietro,⁴⁷ R. de Sangro,⁴¹ B. Deschamps,¹¹⁰ M. Destefanis,^{104,48} S. Dey,⁹³ A. De Yta-Hernandez,⁶ A. Di Canto,³ F. Di Capua,^{99,42} S. Di Carlo,¹⁰⁷ J. Dingfelder,¹¹⁰ Z. Doležal,⁷ I. Domínguez Jiménez,⁹⁸ T. V. Dong,¹⁴ K. Dort,⁵² D. Dossett,¹²⁰ S. Dubey,¹¹⁴ S. Duell,¹¹⁰ G. Dujany,¹⁰⁸ S. Eidelman,^{4,60,77} M. Eliachevitch,¹¹⁰ D. Epifanov,^{4,77} J. E. Fast,⁸¹ T. Ferber,¹² D. Ferlewicz,¹²⁰ T. Fillinger,¹⁰⁸ G. Finocchiaro,⁴¹ S. Fiore,⁴⁶ P. Fischer,¹¹⁵ A. Fodor,⁶⁷ F. Forti,^{102,45} A. Frey,²⁰ M. Friedl,³⁵ B. G. Fulsom,⁸¹ M. Gabriel,⁶⁵ N. Gabyshev,^{4,77} E. Ganiev,^{105,49} M. Garcia-Hernandez,⁶ R. Garg,⁸² A. Garmash,^{4,77} V. Gaur,¹³¹ A. Gaz,^{100,43} U. Gebauer,²⁰ M. Gelb,⁵³ A. Gellrich,¹² J. Gemmler,⁵³ T. Geßler,⁵² D. Getzkow,⁵² R. Giordano,^{99,42} A. Giri,³¹ A. Glazov,¹² B. Gobbo,⁴⁹ R. Godang,¹²⁵ P. Goldenzweig,⁵³ B. Golob,^{116,89} P. Gomis,⁴⁰ P. Grace,¹⁰⁹ W. Gradl,⁵¹ E. Graziani,⁴⁷ D. Greenwald,⁹² Y. Guan,¹¹² K. Gudkova,^{4,77} C. Hadjivasiliou,⁸¹ S. Halder,⁹¹ K. Hara,^{25,22} T. Hara,^{25,22} O. Hartbrich,¹¹⁴ K. Hayasaka,⁷⁶ H. Hayashii,⁷² S. Hazra,⁹¹ C. Hearty,^{111,38} M. T. Hedges,¹¹⁴ I. Heredia de la Cruz,^{6,11} M. Hernández Villanueva,¹²¹ A. Hershenhorn,¹¹¹ T. Higuchi,¹²⁹ E. C. Hill,¹¹¹ H. Hirata,⁶⁹ M. Hoek,⁵¹ M. Hohmann,¹²⁰ S. Hollitt,¹⁰⁹ T. Hotta,⁸⁰ C.-L. Hsu,¹²⁷ Y. Hu,³⁷ K. Huang,⁷³ T. Humair,⁶⁵ T. Iijima,^{69,71} K. Inami,⁶⁹ G. Inguglia,³⁵ J. Irakkathil Jabbar,⁵³ A. Ishikawa,^{25,22} R. Itoh,^{25,22} M. Iwasaki,⁷⁹ Y. Iwasaki,²⁵ S. Iwata,⁹⁷ P. Jackson,¹⁰⁹ W. W. Jacobs,³³ I. Jaegle,¹¹³ D. E. Jaffe,³ E.-J. Jang,²³ M. Jeandron,¹²¹

- H. B. Jeon,⁵⁹ S. Jia,¹⁹ Y. Jin,⁴⁹ C. Joo,¹²⁹ K. K. Joo,¹⁰ H. Junkerkalefeld,¹¹⁰ I. Kadenko,⁹⁰
 J. Kahn,⁵³ H. Kakuno,⁹⁷ A. B. Kaliyar,⁹¹ J. Kandra,⁷ K. H. Kang,⁵⁹ P. Kapusta,⁷⁵
 R. Karl,¹² G. Karyan,¹³⁴ Y. Kato,^{69,71} H. Kawai,⁹ T. Kawasaki,⁵⁵ T. Keck,⁵³ C. Ketter,¹¹⁴
 H. Kichimi,²⁵ C. Kiesling,⁶⁵ B. H. Kim,⁸⁵ C.-H. Kim,²⁴ D. Y. Kim,⁸⁸ H. J. Kim,⁵⁹
 K.-H. Kim,¹³⁵ K. Kim,⁵⁷ S.-H. Kim,⁸⁵ Y.-K. Kim,¹³⁵ Y. Kim,⁵⁷ T. D. Kimmel,¹³¹
 H. Kindo,^{25,22} K. Kinoshita,¹¹² B. Kirby,³ C. Kleinwort,¹² B. Knysh,¹⁰⁷ P. Kodyš,⁷
 T. Koga,²⁵ S. Kohani,¹¹⁴ I. Komarov,¹² T. Konno,⁵⁵ A. Korobov,^{4,77} S. Korpar,^{119,89}
 N. Kovalchuk,¹² E. Kovalenko,^{4,77} T. M. G. Kraetzschmar,⁶⁵ F. Krinner,⁶⁵
 P. Križan,^{116,89} R. Kroeger,¹²¹ J. F. Krohn,¹²⁰ P. Krokovny,^{4,77} H. Krüger,¹¹⁰
 W. Kuehn,⁵² T. Kuhr,⁶² J. Kumar,⁵ M. Kumar,⁶⁴ R. Kumar,⁸³ K. Kumara,¹³²
 T. Kumita,⁹⁷ T. Kunigo,²⁵ M. Künzel,^{12,62} S. Kurz,¹² A. Kuzmin,^{4,77} P. Kvasnička,⁷
 Y.-J. Kwon,¹³⁵ S. Lacaprara,⁴³ Y.-T. Lai,¹²⁹ C. La Licata,¹²⁹ K. Lalwani,⁶⁴ L. Lanceri,⁴⁹
 J. S. Lange,⁵² M. Laurenza,^{103,47} K. Lautenbach,⁵² P. J. Laycock,³ F. R. Le Diberder,¹⁰⁷
 I.-S. Lee,²⁴ S. C. Lee,⁵⁹ P. Leitl,⁶⁵ D. Levit,⁹² P. M. Lewis,¹¹⁰ C. Li,⁶¹ C.-H. Li,⁷³
 L. K. Li,¹¹² S. X. Li,¹⁹ Y. B. Li,¹⁹ J. Libby,³² K. Lieret,⁶² L. Li Gioi,⁶⁵ J. Lin,⁷³
 Z. Liptak,³⁶ Q. Y. Liu,¹² Z. A. Liu,³⁷ D. Liventsev,^{132,25} S. Longo,¹² A. Loos,¹²⁶ P. Lu,⁷³
 M. Lubej,⁸⁹ T. Lueck,⁶² F. Luetticke,¹¹⁰ T. Luo,¹⁹ C. Lyu,¹¹⁰ C. MacQueen,¹²⁰
 Y. Maeda,^{69,71} M. Maggiora,^{104,48} S. Maity,²⁹ R. Manfredi,^{105,49} E. Manoni,⁴⁴
 S. Marcello,^{104,48} C. Marinas,⁴⁰ A. Martini,^{103,47} M. Masuda,^{16,80} T. Matsuda,¹²²
 K. Matsuoka,²⁵ D. Matvienko,^{4,60,77} J. McNeil,¹¹³ F. Meggendorfer,⁶⁵ J. C. Mei,¹⁹
 F. Meier,¹³ M. Merola,^{99,42} F. Metzner,⁵³ M. Milesi,¹²⁰ C. Miller,¹³⁰ K. Miyabayashi,⁷²
 H. Miyake,^{25,22} H. Miyata,⁷⁶ R. Mizuk,^{60,27} K. Azmi,¹¹⁸ G. B. Mohanty,⁹¹ H. Moon,⁵⁷
 T. Moon,⁸⁵ J. A. Mora Grimaldo,¹²⁸ T. Morii,¹²⁹ H.-G. Moser,⁶⁵ M. Mrvar,³⁵
 F. Mueller,⁶⁵ F. J. Müller,¹² Th. Muller,⁵³ G. Muroyama,⁶⁹ C. Murphy,¹²⁹ R. Mussa,⁴⁸
 K. Nakagiri,²⁵ I. Nakamura,^{25,22} K. R. Nakamura,^{25,22} E. Nakano,⁷⁹ M. Nakao,^{25,22}
 H. Nakayama,^{25,22} H. Nakazawa,⁷³ T. Nanut,⁸⁹ Z. Natkaniec,⁷⁵ A. Natochii,¹¹⁴
 M. Nayak,⁹³ G. Nazaryan,¹³⁴ D. Neverov,⁶⁹ C. Niebuhr,¹² M. Niijima,⁵⁸ J. Ninkovic,⁶⁶
 N. K. Nisar,³ S. Nishida,^{25,22} K. Nishimura,¹¹⁴ M. Nishimura,²⁵ M. H. A. Nouxman,¹¹⁸
 B. Oberhof,⁴¹ K. Ogawa,⁷⁶ S. Ogawa,⁹⁴ S. L. Olsen,²³ Y. Onishchuk,⁹⁰ H. Ono,⁷⁶
 Y. Onuki,¹²⁸ P. Oskin,⁶⁰ E. R. Oxford,⁵ H. Ozaki,^{25,22} P. Pakhlov,^{60,68} G. Pakhlova,^{27,60}
 A. Paladino,^{102,45} T. Pang,¹²³ A. Panta,¹²¹ E. Paoloni,^{102,45} S. Pardi,⁴² H. Park,⁵⁹
 S.-H. Park,²⁵ B. Paschen,¹¹⁰ A. Passeri,⁴⁷ A. Pathak,¹¹⁷ S. Patra,²⁸ S. Paul,⁹²
 T. K. Pedlar,⁶³ I. Peruzzi,⁴¹ R. Peschke,¹¹⁴ R. Pestotnik,⁸⁹ M. Piccolo,⁴¹ L. E. Piilonen,¹³¹
 P. L. M. Podesta-Lerma,⁹⁸ G. Polat,¹ V. Popov,²⁷ C. Praz,¹² S. Prell,⁵⁴ E. Prencipe,¹⁷
 M. T. Prim,¹¹⁰ M. V. Purohit,⁷⁸ N. Rad,¹² P. Rados,¹² S. Raiz,^{105,49} R. Rasheed,¹⁰⁸
 M. Reif,⁶⁵ S. Reiter,⁵² M. Remnev,^{4,77} P. K. Resmi,³² I. Ripp-Baudot,¹⁰⁸ M. Ritter,⁶²
 M. Ritzert,¹¹⁵ G. Rizzo,^{102,45} L. B. Rizzuto,⁸⁹ S. H. Robertson,^{67,38} D. Rodríguez Pérez,⁹⁸
 J. M. Roney,^{130,38} C. Rosenfeld,¹²⁶ A. Rostomyan,¹² N. Rout,³² M. Rozanska,⁷⁵
 G. Russo,^{99,42} D. Sahoo,⁹¹ Y. Sakai,^{25,22} D. A. Sanders,¹²¹ S. Sandilya,³¹ A. Sangal,¹¹²
 L. Santelj,^{116,89} P. Sartori,^{100,43} J. Sasaki,¹²⁸ Y. Sato,⁹⁵ V. Savinov,¹²³ B. Scavino,⁵¹
 M. Schram,⁸¹ H. Schreeck,²⁰ J. Schueler,¹¹⁴ C. Schwanda,³⁵ A. J. Schwartz,¹¹²
 B. Schwenker,²⁰ R. M. Seddon,⁶⁷ Y. Seino,⁷⁶ A. Selce,^{47,15} K. Senyo,¹³³ I. S. Seong,¹¹⁴
 J. Serrano,¹ M. E. Sevior,¹²⁰ C. Sfienti,⁵¹ V. Shebalin,¹¹⁴ C. P. Shen,² H. Shibuya,⁹⁴
 J.-G. Shiu,⁷³ B. Shwartz,^{4,77} A. Sibidanov,¹¹⁴ F. Simon,⁶⁵ J. B. Singh,⁸² S. Skambraks,⁶⁵

K. Smith,¹²⁰ R. J. Sobie,^{130,38} A. Soffer,⁹³ A. Sokolov,³⁴ Y. Soloviev,¹² E. Solovieva,⁶⁰
 S. Spataro,^{104,48} B. Spruck,⁵¹ M. Starič,⁸⁹ S. Stefkova,¹² Z. S. Stottler,¹³¹ R. Stroili,^{100,43}
 J. Strube,⁸¹ J. Stypula,⁷⁵ M. Sumihama,^{21,80} K. Sumisawa,^{25,22} T. Sumiyoshi,⁹⁷
 D. J. Summers,¹²¹ W. Sutcliffe,¹¹⁰ K. Suzuki,⁶⁹ S. Y. Suzuki,^{25,22} H. Svidras,¹² M. Tabata,⁹
 M. Takahashi,¹² M. Takizawa,^{84,26,86} U. Tamponi,⁴⁸ S. Tanaka,^{25,22} K. Tanida,⁵⁰
 H. Tanigawa,¹²⁸ N. Taniguchi,²⁵ Y. Tao,¹¹³ P. Taras,¹⁰⁶ F. Tenchini,¹² D. Tonelli,⁴⁹
 E. Torassa,⁴³ K. Trabelsi,¹⁰⁷ T. Tsuboyama,^{25,22} N. Tsuzuki,⁶⁹ M. Uchida,⁹⁶ I. Ueda,^{25,22}
 S. Uehara,^{25,22} T. Ueno,⁹⁵ T. Uglov,^{60,27} K. Unger,⁵³ Y. Unno,²⁴ S. Uno,^{25,22} P. Urquijo,¹²⁰
 Y. Ushiroda,^{25,22,128} Y. V. Usov,^{4,77} S. E. Vahsen,¹¹⁴ R. van Tonder,¹¹⁰ G. S. Varner,¹¹⁴
 K. E. Varvell,¹²⁷ A. Vinokurova,^{4,77} L. Vitale,^{105,49} V. Vorobyev,^{4,60,77} A. Vossen,¹³
 B. Wach,⁶⁵ E. Waheed,²⁵ H. M. Wakeling,⁶⁷ K. Wan,¹²⁸ W. Wan Abdullah,¹¹⁸ B. Wang,⁶⁵
 C. H. Wang,⁷⁴ M.-Z. Wang,⁷³ X. L. Wang,¹⁹ A. Warburton,⁶⁷ M. Watanabe,⁷⁶
 S. Watanuki,¹⁰⁷ J. Webb,¹²⁰ S. Wehle,¹² M. Welsch,¹¹⁰ C. Wessel,¹¹⁰ J. Wiechczynski,⁴⁵
 P. Wieduwilt,²⁰ H. Windel,⁶⁵ E. Won,⁵⁷ L. J. Wu,³⁷ X. P. Xu,⁸⁷ B. D. Yabsley,¹²⁷
 S. Yamada,²⁵ W. Yan,¹²⁴ S. B. Yang,⁵⁷ H. Ye,¹² J. Yelton,¹¹³ I. Yeo,⁵⁶ J. H. Yin,⁵⁷
 M. Yonenaga,⁹⁷ Y. M. Yook,³⁷ K. Yoshihara,⁵⁴ T. Yoshinobu,⁷⁶ C. Z. Yuan,³⁷ G. Yuan,¹²⁴
 Y. Yusa,⁷⁶ L. Zani,¹ J. Z. Zhang,³⁷ Y. Zhang,¹²⁴ Z. Zhang,¹²⁴ V. Zhilich,^{4,77} J. Zhou,¹⁹
 Q. D. Zhou,^{69,70,71} X. Y. Zhou,⁶¹ V. I. Zhukova,⁶⁰ V. Zhulanov,^{4,77} and A. Zupanc⁸⁹

¹*Aix Marseille Université, CNRS/IN2P3, CPPM, 13288 Marseille, France*

²*Beihang University, Beijing 100191, China*

³*Brookhaven National Laboratory, Upton, New York 11973, U.S.A.*

⁴*Budker Institute of Nuclear Physics SB RAS, Novosibirsk 630090, Russian Federation*

⁵*Carnegie Mellon University, Pittsburgh, Pennsylvania 15213, U.S.A.*

⁶*Centro de Investigacion y de Estudios Avanzados del
Instituto Politecnico Nacional, Mexico City 07360, Mexico*

⁷*Faculty of Mathematics and Physics, Charles University, 121 16 Prague, Czech Republic*

⁸*Chiang Mai University, Chiang Mai 50202, Thailand*

⁹*Chiba University, Chiba 263-8522, Japan*

¹⁰*Chonnam National University, Gwangju 61186, South Korea*

¹¹*Consejo Nacional de Ciencia y Tecnología, Mexico City 03940, Mexico*

¹²*Deutsches Elektronen-Synchrotron, 22607 Hamburg, Germany*

¹³*Duke University, Durham, North Carolina 27708, U.S.A.*

¹⁴*Institute of Theoretical and Applied Research
(ITAR), Duy Tan University, Hanoi 100000, Vietnam*

¹⁵*ENEA Casaccia, I-00123 Roma, Italy*

¹⁶*Earthquake Research Institute, University of Tokyo, Tokyo 113-0032, Japan*

¹⁷*Forschungszentrum Jülich, 52425 Jülich, Germany*

¹⁸*Department of Physics, Fu Jen Catholic University, Taipei 24205, Taiwan*

¹⁹*Key Laboratory of Nuclear Physics and Ion-beam Application (MOE) and
Institute of Modern Physics, Fudan University, Shanghai 200443, China*

²⁰*II. Physikalisches Institut, Georg-August-Universität
Göttingen, 37073 Göttingen, Germany*

²¹*Gifu University, Gifu 501-1193, Japan*

²²*The Graduate University for Advanced Studies (SOKENDAI), Hayama 240-0193, Japan*

²³*Gyeongsang National University, Jinju 52828, South Korea*

- ²⁴*Department of Physics and Institute of Natural Sciences, Hanyang University, Seoul 04763, South Korea*
- ²⁵*High Energy Accelerator Research Organization (KEK), Tsukuba 305-0801, Japan*
- ²⁶*J-PARC Branch, KEK Theory Center, High Energy Accelerator Research Organization (KEK), Tsukuba 305-0801, Japan*
- ²⁷*National Research University Higher School of Economics, Moscow 101000, Russian Federation*
- ²⁸*Indian Institute of Science Education and Research Mohali, SAS Nagar, 140306, India*
- ²⁹*Indian Institute of Technology Bhubaneswar, Satya Nagar 751007, India*
- ³⁰*Indian Institute of Technology Guwahati, Assam 781039, India*
- ³¹*Indian Institute of Technology Hyderabad, Telangana 502285, India*
- ³²*Indian Institute of Technology Madras, Chennai 600036, India*
- ³³*Indiana University, Bloomington, Indiana 47408, U.S.A.*
- ³⁴*Institute for High Energy Physics, Protvino 142281, Russian Federation*
- ³⁵*Institute of High Energy Physics, Vienna 1050, Austria*
- ³⁶*Hiroshima University, Higashi-Hiroshima, Hiroshima 739-8530, Japan*
- ³⁷*Institute of High Energy Physics, Chinese Academy of Sciences, Beijing 100049, China*
- ³⁸*Institute of Particle Physics (Canada), Victoria, British Columbia V8W 2Y2, Canada*
- ³⁹*Institute of Physics, Vietnam Academy of Science and Technology (VAST), Hanoi, Vietnam*
- ⁴⁰*Instituto de Fisica Corpuscular, Paterna 46980, Spain*
- ⁴¹*INFN Laboratori Nazionali di Frascati, I-00044 Frascati, Italy*
- ⁴²*INFN Sezione di Napoli, I-80126 Napoli, Italy*
- ⁴³*INFN Sezione di Padova, I-35131 Padova, Italy*
- ⁴⁴*INFN Sezione di Perugia, I-06123 Perugia, Italy*
- ⁴⁵*INFN Sezione di Pisa, I-56127 Pisa, Italy*
- ⁴⁶*INFN Sezione di Roma, I-00185 Roma, Italy*
- ⁴⁷*INFN Sezione di Roma Tre, I-00146 Roma, Italy*
- ⁴⁸*INFN Sezione di Torino, I-10125 Torino, Italy*
- ⁴⁹*INFN Sezione di Trieste, I-34127 Trieste, Italy*
- ⁵⁰*Advanced Science Research Center, Japan Atomic Energy Agency, Naka 319-1195, Japan*
- ⁵¹*Johannes Gutenberg-Universität Mainz, Institut für Kernphysik, D-55099 Mainz, Germany*
- ⁵²*Justus-Liebig-Universität Gießen, 35392 Gießen, Germany*
- ⁵³*Institut für Experimentelle Teilchenphysik, Karlsruher Institut für Technologie, 76131 Karlsruhe, Germany*
- ⁵⁴*Iowa State University, Ames, Iowa 50011, U.S.A.*
- ⁵⁵*Kitasato University, Sagamihara 252-0373, Japan*
- ⁵⁶*Korea Institute of Science and Technology Information, Daejeon 34141, South Korea*
- ⁵⁷*Korea University, Seoul 02841, South Korea*
- ⁵⁸*Kyoto Sangyo University, Kyoto 603-8555, Japan*
- ⁵⁹*Kyungpook National University, Daegu 41566, South Korea*
- ⁶⁰*P.N. Lebedev Physical Institute of the Russian Academy of Sciences, Moscow 119991, Russian Federation*
- ⁶¹*Liaoning Normal University, Dalian 116029, China*
- ⁶²*Ludwig Maximilians University, 80539 Munich, Germany*
- ⁶³*Luther College, Decorah, Iowa 52101, U.S.A.*

- ⁶⁴Malaviya National Institute of Technology Jaipur, Jaipur 302017, India
⁶⁵Max-Planck-Institut für Physik, 80805 München, Germany
⁶⁶Semiconductor Laboratory of the Max Planck Society, 81739 München, Germany
⁶⁷McGill University, Montréal, Québec, H3A 2T8, Canada
⁶⁸Moscow Physical Engineering Institute, Moscow 115409, Russian Federation
⁶⁹Graduate School of Science, Nagoya University, Nagoya 464-8602, Japan
⁷⁰Institute for Advanced Research, Nagoya University, Nagoya 464-8602, Japan
⁷¹Kobayashi-Maskawa Institute, Nagoya University, Nagoya 464-8602, Japan
⁷²Nara Women's University, Nara 630-8506, Japan
⁷³Department of Physics, National Taiwan University, Taipei 10617, Taiwan
⁷⁴National United University, Miao Li 36003, Taiwan
⁷⁵H. Niewodniczanski Institute of Nuclear Physics, Krakow 31-342, Poland
⁷⁶Niigata University, Niigata 950-2181, Japan
⁷⁷Novosibirsk State University, Novosibirsk 630090, Russian Federation
⁷⁸Okinawa Institute of Science and Technology, Okinawa 904-0495, Japan
⁷⁹Osaka City University, Osaka 558-8585, Japan
⁸⁰Research Center for Nuclear Physics, Osaka University, Osaka 567-0047, Japan
⁸¹Pacific Northwest National Laboratory, Richland, Washington 99352, U.S.A.
⁸²Panjab University, Chandigarh 160014, India
⁸³Punjab Agricultural University, Ludhiana 141004, India
⁸⁴Meson Science Laboratory, Cluster for Pioneering
Research, RIKEN, Saitama 351-0198, Japan
⁸⁵Seoul National University, Seoul 08826, South Korea
⁸⁶Showa Pharmaceutical University, Tokyo 194-8543, Japan
⁸⁷Soochow University, Suzhou 215006, China
⁸⁸Soongsil University, Seoul 06978, South Korea
⁸⁹J. Stefan Institute, 1000 Ljubljana, Slovenia
⁹⁰Taras Shevchenko National Univ. of Kiev, Kiev, Ukraine
⁹¹Tata Institute of Fundamental Research, Mumbai 400005, India
⁹²Department of Physics, Technische Universität München, 85748 Garching, Germany
⁹³Tel Aviv University, School of Physics and Astronomy, Tel Aviv, 69978, Israel
⁹⁴Toho University, Funabashi 274-8510, Japan
⁹⁵Department of Physics, Tohoku University, Sendai 980-8578, Japan
⁹⁶Tokyo Institute of Technology, Tokyo 152-8550, Japan
⁹⁷Tokyo Metropolitan University, Tokyo 192-0397, Japan
⁹⁸Universidad Autonoma de Sinaloa, Sinaloa 80000, Mexico
⁹⁹Dipartimento di Scienze Fisiche, Università di Napoli Federico II, I-80126 Napoli, Italy
¹⁰⁰Dipartimento di Fisica e Astronomia, Università di Padova, I-35131 Padova, Italy
¹⁰¹Dipartimento di Fisica, Università di Perugia, I-06123 Perugia, Italy
¹⁰²Dipartimento di Fisica, Università di Pisa, I-56127 Pisa, Italy
¹⁰³Dipartimento di Matematica e Fisica, Università di Roma Tre, I-00146 Roma, Italy
¹⁰⁴Dipartimento di Fisica, Università di Torino, I-10125 Torino, Italy
¹⁰⁵Dipartimento di Fisica, Università di Trieste, I-34127 Trieste, Italy
¹⁰⁶Université de Montréal, Physique des Particules, Montréal, Québec, H3C 3J7, Canada
¹⁰⁷Université Paris-Saclay, CNRS/IN2P3, IJCLab, 91405 Orsay, France
¹⁰⁸Université de Strasbourg, CNRS, IPHC, UMR 7178, 67037 Strasbourg, France
¹⁰⁹Department of Physics, University of Adelaide, Adelaide, South Australia 5005, Australia

- ¹¹⁰*University of Bonn, 53115 Bonn, Germany*
- ¹¹¹*University of British Columbia, Vancouver, British Columbia, V6T 1Z1, Canada*
- ¹¹²*University of Cincinnati, Cincinnati, Ohio 45221, U.S.A.*
- ¹¹³*University of Florida, Gainesville, Florida 32611, U.S.A.*
- ¹¹⁴*University of Hawaii, Honolulu, Hawaii 96822, U.S.A.*
- ¹¹⁵*University of Heidelberg, 68131 Mannheim, Germany*
- ¹¹⁶*Faculty of Mathematics and Physics, University of Ljubljana, 1000 Ljubljana, Slovenia*
- ¹¹⁷*University of Louisville, Louisville, Kentucky 40292, U.S.A.*
- ¹¹⁸*National Centre for Particle Physics, University Malaya, 50603 Kuala Lumpur, Malaysia*
- ¹¹⁹*Faculty of Chemistry and Chemical Engineering,
University of Maribor, 2000 Maribor, Slovenia*
- ¹²⁰*School of Physics, University of Melbourne, Victoria 3010, Australia*
- ¹²¹*University of Mississippi, University, Mississippi 38677, U.S.A.*
- ¹²²*University of Miyazaki, Miyazaki 889-2192, Japan*
- ¹²³*University of Pittsburgh, Pittsburgh, Pennsylvania 15260, U.S.A.*
- ¹²⁴*University of Science and Technology of China, Hefei 230026, China*
- ¹²⁵*University of South Alabama, Mobile, Alabama 36688, U.S.A.*
- ¹²⁶*University of South Carolina, Columbia, South Carolina 29208, U.S.A.*
- ¹²⁷*School of Physics, University of Sydney, New South Wales 2006, Australia*
- ¹²⁸*Department of Physics, University of Tokyo, Tokyo 113-0033, Japan*
- ¹²⁹*Kavli Institute for the Physics and Mathematics of the
Universe (WPI), University of Tokyo, Kashiwa 277-8583, Japan*
- ¹³⁰*University of Victoria, Victoria, British Columbia, V8W 3P6, Canada*
- ¹³¹*Virginia Polytechnic Institute and State University, Blacksburg, Virginia 24061, U.S.A.*
- ¹³²*Wayne State University, Detroit, Michigan 48202, U.S.A.*
- ¹³³*Yamagata University, Yamagata 990-8560, Japan*
- ¹³⁴*Alikhanyan National Science Laboratory, Yerevan 0036, Armenia*
- ¹³⁵*Yonsei University, Seoul 03722, South Korea*
- ¹³⁶*Zhengzhou University, Zhengzhou 450001, China*

Abstract

We report measurements of branching fractions (\mathcal{B}) and direct CP -violating asymmetries (\mathcal{A}_{CP}) for the decays $B^+ \rightarrow K^+\pi^0$ and $B^+ \rightarrow \pi^+\pi^0$ reconstructed with the Belle II detector in a sample of asymmetric-energy electron-positron collisions at the $\Upsilon(4S)$ resonance corresponding to 62.8 fb^{-1} of integrated luminosity. The results are $\mathcal{B}(B^+ \rightarrow K^+\pi^0) = [11.9^{+1.1}_{-1.0}(\text{stat}) \pm 1.6(\text{syst})] \times 10^{-6}$, $\mathcal{B}(B^+ \rightarrow \pi^+\pi^0) = [5.5^{+1.0}_{-0.9}(\text{stat}) \pm 0.7(\text{syst})] \times 10^{-6}$, $\mathcal{A}_{CP}(B^+ \rightarrow K^+\pi^0) = -0.09 \pm 0.09(\text{stat}) \pm 0.03(\text{syst})$, and $\mathcal{A}_{CP}(B^+ \rightarrow \pi^+\pi^0) = -0.04 \pm 0.17(\text{stat}) \pm 0.06(\text{syst})$. The results are consistent with previous measurements and show a detector performance comparable with early Belle performance.

1. INTRODUCTION AND MOTIVATION

The study of charmless B decays is a keystone of the worldwide flavor program. Processes mediated by $b \rightarrow sq\bar{q}$ transitions probe contributions of non-standard-model dynamics in loop decay-amplitudes. However, reliable extraction of weak phases and unambiguous interpretation of measurements involving these amplitudes is spoiled by large hadronic uncertainties, which are rarely tractable in perturbative calculations. Appropriately chosen combinations of measurements from decay modes related by flavor symmetries are used to significantly reduce the impact of such unknowns. An especially fruitful approach consists in combining measurements from decays related by isospin symmetries. This approach has been proposed to address the so-called $K\pi$ *puzzle*, a long-standing anomaly associated with the significant difference between direct CP -violating asymmetries observed in $B^0 \rightarrow K^+\pi^-$ and $B^+ \rightarrow K^+\pi^0$ decays [1]. The asymmetries are expected to be equal at leading order in electroweak perturbation theory, as the two decays differ only by the *spectator* quark. The isospin sum-rule

$$I_{K\pi} = \mathcal{A}_{K^+\pi^-} + \mathcal{A}_{K^0\pi^+} \frac{\mathcal{B}(K^0\pi^+)}{\mathcal{B}(K^+\pi^-)} \frac{\tau_{B^0}}{\tau_{B^+}} - 2\mathcal{A}_{K^+\pi^0} \frac{\mathcal{B}(K^+\pi^0)}{\mathcal{B}(K^+\pi^-)} \frac{\tau_{B^0}}{\tau_{B^+}} - 2\mathcal{A}_{K^0\pi^0} \frac{\mathcal{B}(K^0\pi^0)}{\mathcal{B}(K^+\pi^-)}, \quad (1)$$

properly accounts for subleading amplitudes by combining the branching fractions (\mathcal{B}) and direct CP asymmetries (\mathcal{A}) of $B^+(B^0)$ decays to all four final states $K^+\pi^-$, $K^0\pi^+$, $K^+\pi^0$, and $K^0\pi^0$, and the lifetime (τ) ratio between B^+ and B^0 . This rule offers a stringent null test of the standard model (SM), which predicts $I_{K\pi} = 0$ in the limit of exact isospin symmetry and no electroweak penguin (EWP) contributions, and with an uncertainty much below 1% when including SM EWP amplitudes [2, 3]. For $B^+ \rightarrow \pi^+\pi^0$ decay, the branching fraction is an ingredient (Figure 1) for an isospin-based determination of α/ϕ_2 based on $B \rightarrow \pi\pi$ decays [4]. Belle II has the unique capability of studying jointly, and within a consistent experimental environment, all relevant final states.

The Belle II experiment, complete with its vertex detector, started its collision operations in March 2019 and is currently collecting data. The sample of electron-positron collisions used in this work corresponds to an integrated luminosity of 62.8 fb^{-1} and was collected at the $\Upsilon(4S)$ resonance.

We report updated Belle II measurements of branching fractions and direct CP -violating asymmetries in $B^+ \rightarrow K^+\pi^0$ and $B^+ \rightarrow \pi^+\pi^0$ decays. These results supersede those in Ref [5] using more data and an improved analysis. All analysis procedures are first developed and finalized in simulated data and then tested on the data used for summer 2020 results [5] prior to the application on the full data set.

2. THE BELLE II DETECTOR

Belle II is a 4π particle-physics spectrometer [6, 7], designed to reconstruct the products of electron-positron collisions produced by the SuperKEKB asymmetric-energy collider [8], located at the KEK laboratory in Tsukuba, Japan. Belle II comprises several subdetectors arranged around the interaction space-point in a cylindrical geometry. The innermost subdetector is the vertex detector, which uses position-sensitive silicon layers to sample the trajectories of charged particles (tracks) in the vicinity of the interaction region in order to extrapolate the decay positions of their long-lived parent particles. The vertex detector includes

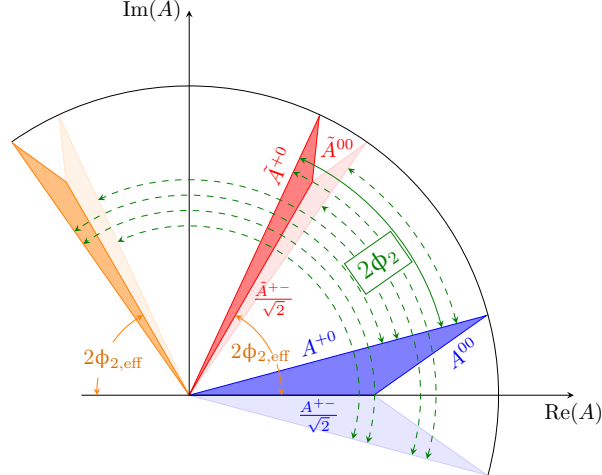


FIG. 1. Geometrical representation of the isospin triangular relations in the complex plane of $B^{i+j} \rightarrow h^i h^j$ amplitudes (A^{ij}). The blue and the red shaded areas correspond to the isospin triangles. The angle between the CP conjugate charged amplitudes A^{+-} and \tilde{A}^{+-} corresponds to twice the weak phase $\alpha_{\text{eff}}/\phi_{2,\text{eff}}$ (orange solid curves). The angle between the CP conjugate charged amplitudes A^{+0} and \tilde{A}^{+0} corresponds to twice the CKM angle α/ϕ_2 (green solid curve). The other triangles with lighter shades represent the mirror solutions allowed by the discrete ambiguities associated with the isospin relationships, with the corresponding values for α/ϕ_2 represented by the green dashed curves.

two inner layers of silicon pixel sensors and four outer layers of silicon microstrip sensors. The second pixel layer is currently incomplete and covers only a small portion of azimuthal angle. Charged-particle momenta and charges are measured by a large-radius, helium-ethane, small-cell central drift chamber, which also offers charged-particle-identification information through a measurement of particles' energy-loss by specific ionization. A Cherenkov-light angle and time-of-propagation detector surrounding the chamber provides charged-particle identification in the central detector volume, supplemented by proximity-focusing, aerogel, ring-imaging Cherenkov detectors in the forward regions. A CsI(Tl)-crystal electromagnetic calorimeter allows for energy measurements of electrons and photons. A solenoid surrounding the calorimeter generates a uniform axial 1.5 T magnetic field filling its inner volume. Layers of plastic scintillator and resistive-plate chambers, interspersed between the magnetic flux-return iron plates, allow for identification of K_L^0 and muons. The subdetectors most relevant for this work are the silicon vertex detector, the tracking drift chamber, the particle-identification detectors, and the electromagnetic calorimeter.

3. DATA AND SIMULATION

We use all 2019–2020 $\Upsilon(4S)$ collected on $\Upsilon(4S)$ resonance until July 1, 2020 corresponding to an integrated luminosity of 62.8 fb^{-1} . All events are required to satisfy initial loose data-skim selections, based on total energy and charged-particle multiplicity in the event, targeted at reducing sample sizes to a manageable level with negligible impact on signal efficiency. All data are processed using the Belle II analysis software [9].

We use generic simulated data to optimize the event selection and compare the distribu-

tions observed in experimental data with expectations. We use signal-only simulated data to model relevant signal features for fits and determine selection efficiencies. Generic simulation consists of Monte Carlo samples that include $B^0\bar{B}^0$, B^+B^- , $u\bar{u}$, $d\bar{d}$, $s\bar{s}$, and $c\bar{c}$ processes in realistic proportions and corresponding in size to more than ten times the experimental data.

4. EVENT SELECTION AND CANDIDATE RECONSTRUCTION

Candidate charged particles are required to be reconstructed in the full polar-angle acceptance ($17^\circ < \theta < 150^\circ$) and originate at the interaction point with longitudinal displacement $|dz| < 3.0$ cm and radial displacement $|dr| < 0.5$ cm to reduce beam-background-induced tracks. Charged kaons and pions are identified using the dE/dx information from the drift chamber and particle identification in the Cherenkov detectors. For a 2 GeV/c charged kaon/pion, the identification efficiency is 88%/91% while 9%/11% pions/kaons are misidentified as kaons/pions. Candidate neutral pions are reconstructed in their diphoton decays. Photon pairs with masses between 0.105 and 0.150 GeV/ c^2 are selected as π^0 candidates. To reduce the combinatorial background from soft photons, the energy of each candidate photon is required to exceed 22.5 MeV in the forward endcap region and 20 MeV in the barrel and the backward endcap regions. Furthermore, the magnitude of the cosine of the angle between the photon direction in the π^0 rest frame and the π^0 direction in the laboratory frame, is required to be less than 0.98. Photon pairs are kinematically fitted to the known π^0 mass based on their measured energies, directions, and associated covariance matrices.

Candidate B mesons are selected by pairing a charged kaon or pion candidate with a π^0 candidate, and are identified using the energy difference, $\Delta E \equiv E_B^* - E_{\text{beam}}^*$ and the modified beam energy-constrained mass, $M_{bc} \equiv \sqrt{E_{\text{beam}}^{*2}/c^4 - |\vec{p}_{h^\pm}^*/c + \vec{p}^*(\gamma\gamma)_{\pi^0}/c|^2}$ with $\vec{p}^*(\gamma\gamma)_{\pi^0} = \sqrt{(E_{\text{beam}}^{*2}/c^2 - E_{h^\pm}^{*2}/c^2) - (m^*(\gamma\gamma)_{\pi^0}c)^2} \cdot \hat{p}^*(\gamma\gamma)_{\pi^0}$, where E_{beam}^* is the run-dependent beam energy, $m^*(\gamma\gamma)_{\pi^0}$ is the reconstructed mass of π^0 candidates after kinematical fit, and $E_{B(h^\pm)}^*$, $p_{h^\pm}^*$, and $p^*(\gamma\gamma)_{\pi^0}$ are the reconstructed energy and momentum of B , h^\pm , and π^0 candidates in the center-of-mass frame, respectively. B candidates with $M_{bc} > 5.2$ GeV/ c^2 and $|\Delta E| < 0.3$ GeV are retained for further analysis.

5. BACKGROUND REDUCTION

The main challenge in reconstructing charmless B decay is the large contamination from continuum background. We use a binary boosted decision-tree classifier that combines non-linearly 39 variables known to provide statistical discrimination between B -meson signals and continuum background and to be loosely correlated with M_{bc} and ΔE . The variables are quantities associated with event topology (global and signal-only angular configurations), flavor-tagger information, vertex separation and uncertainty information, and kinematic-fit quality information. We train the classifier to identify statistically significant signal and background features using unbiased simulated samples. We validate the input and output distributions of the classifier by comparing control-sample data with simulation. Figure 2 shows the distribution of the output for $B^+ \rightarrow \bar{D}^0(\rightarrow K^+\pi^-)\pi^+$ candidates reconstructed in data and simulation. No inconsistency is observed.

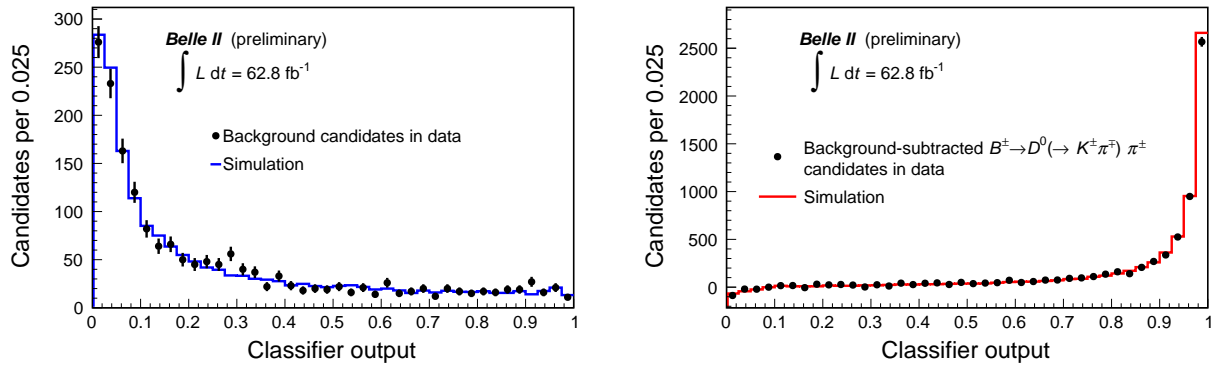


FIG. 2. Data-simulation comparison of the output of the boosted decision-tree classifier on (left) sideband and (right) side-band-subtracted $B^+ \rightarrow \bar{D}^0(\rightarrow K^+ \pi^-) \pi^+$ candidates in the signal region.

To suppress the continuum background effectively, we scan various requirement on the classifier output to search for the criterion that maximises the figure of merit $S/\sqrt{S+B}$, where S and B are the estimated numbers of simulated signal and background candidates in the signal region. The optimal requirement has a signal efficiency and a background retention of 54.6% and 0.7% for the $K^+ \pi^0$ final state, respectively. For the $\pi^+ \pi^0$ final state, the signal efficiency is 44.0%, with 0.4% background retention.

More than one signal candidate is reconstructed in about 5% of events. For those events, we keep only the candidate with the best $h^+ \pi^0$ kinematic-fit quality. A fraction of nonsignal B decays survive the selection, dominated by misidentified $B^+ \rightarrow \pi^+ \pi^0$ and $B^+ \rightarrow K^+ \pi^0$ (feed-across) decays, which are estimated from simulation. Typical feed-across backgrounds have signal-like shapes in M_{bc} and ΔE , except for a ΔE shift due to the incorrect mass assignment.

A significant fraction of background comes from other B decays due to misreconstruction or partial reconstruction of the final state, *e.g.*, $B^0 \rightarrow K^+ \rho^- (\rightarrow \pi^- \pi^0)$ or $B^0 \rightarrow \pi^+ \pi^- \pi^0$. These decays peak like the signal in the M_{bc} distribution and show broader ΔE peaks shifted toward negative values.

6. CORRECTIONS TO SIMULATION FROM CONTROL DATA

We use the decay $B^+ \rightarrow \bar{D}^0(\rightarrow K^+ \pi^- \pi^0) \pi^+$ to study a bias in the photon-energy calibration, which gives a $\mathcal{O}(10)$ MeV shift of the signal peak in the ΔE distribution; we determined corrections for data-simulation discrepancies in the signal shape.

Final-state particle selections similar to that of signal decay are applied, with a stringent requirement on the π^0 momentum (> 1.5 GeV/ c). To select kinematic properties as close as possible to that of the signal π^0 . The correction factors for the simulation are determined by a fit to the M_{bc} and ΔE distribution of the control sample. The signal is modelled with a sum of two Gaussian functions in M_{bc} and a Crystal-Ball function in ΔE . Shape parameters are determined from simulation. Independent mean shifts and width scale-factors for M_{bc} and ΔE are determined from the fit to data as correction factors. From simulation we estimate a 10% fraction of B decay background coming from particle misidentification, which has shapes similar to the signal in M_{bc} and ΔE . The fraction of this background is Gaussian-constrained to its prediction from simulation and known branching fractions. Other B decay

background from partially reconstructed B decays are modelled by using a two-dimensional kernel-density estimator derived from simulation. The continuum background is described by an Argus function in M_{bc} and a second-order polynomial in ΔE .

The resulting difference in the means of ΔE between data and simulation is -17.0 ± 1.4 MeV, and the resulting width scale-factor is about 8% larger in data. We use these corrections in the fit to the signal sample. No data-simulation discrepancy has been observed for the M_{bc} distribution. Figure 3 shows the M_{bc} - ΔE distributions with fit projections overlaid, in the signal region, $M_{bc} > 5.27$ GeV/ c^2 and $-0.14 < \Delta E < 0.06$ GeV.

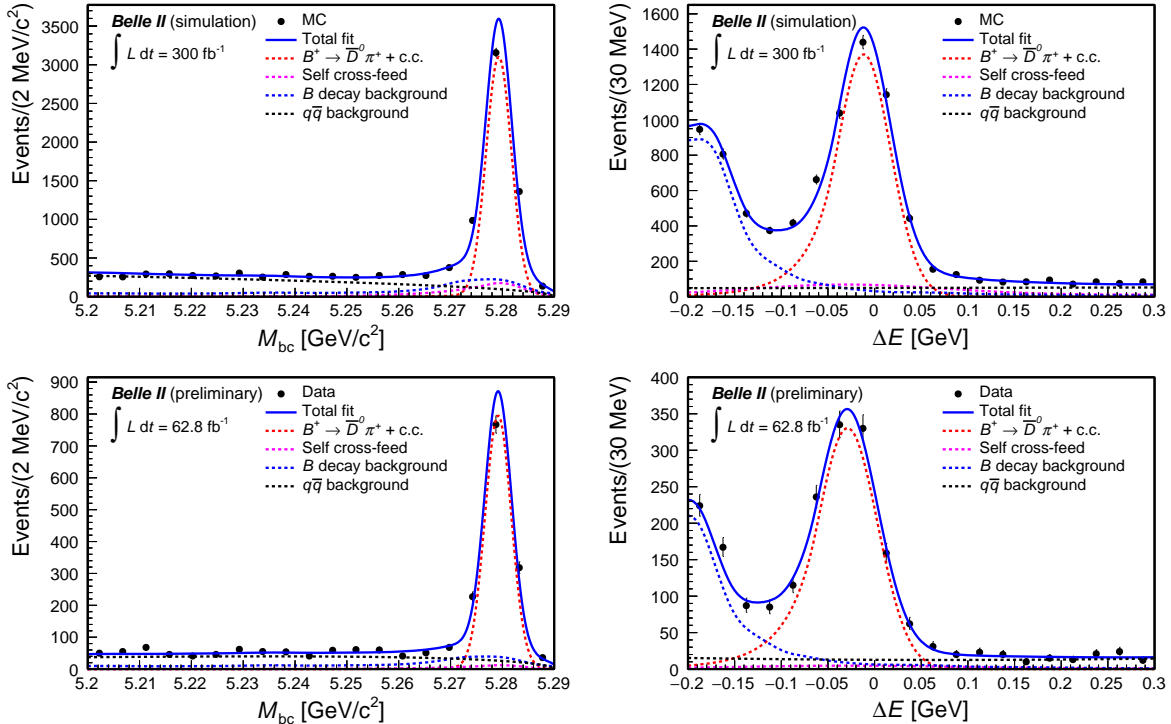


FIG. 3. Distributions of (left) M_{bc} and (right) ΔE for $B^+ \rightarrow \bar{D}^0(\rightarrow K^+\pi^-\pi^0)\pi^+$ candidates reconstructed in (top) simulated events and (bottom) data selected with an optimized continuum-suppression requirement, and projected onto the signal region (left panel: $-0.14 < \Delta E < 0.06$ GeV, right panel: $M_{bc} > 5.27$ GeV/ c^2). The projections of the fit are overlaid.

7. SIGNAL DETERMINATION

The total signal yields and CP -violating charge-asymmetries are obtained using extended maximum-likelihood fits of the M_{bc} and ΔE distributions. The probability density function (PDF) for ΔE is modeled by a Crystal Ball function and a Gaussian function with a common peak position to describe the long tail in the low ΔE region due to photon-shower leakage in the calorimeter. The M_{bc} PDF is described by two Gaussian functions with a common mean. All the PDF parameters are first obtained using the Monte Carlo simulation and then corrected for MC-data discrepancies based on the control sample study described in Section 6. The PDF for the $B\bar{B}$ background is modeled by a two-dimension kernel function, which is a superposition of Gaussian functions for each M_{bc} - ΔE point. The PDF for the

continuum background is modeled as the product of an Argus function in M_{bc} and a second order polynomial in ΔE .

The likelihood function for each mode is

$$L = \frac{e^{-\sum_i N_j}}{N!} \prod_{i=1}^N \left(\sum_i N_j P_j^i(M_{bc}, \Delta E) \right), \text{ where} \\ P_j^i(M_{bc}, \Delta E) = \frac{1}{2}(1 - q_i \cdot \mathcal{A}_{raw}) \times P_j(M_{bc}, \Delta E). \quad (2)$$

Here i is the event index and N_j is the yield of events for the category j , which indexes signal, continuum, feed-across, and other B decays. Here $P_j^i(M_{bc}, \Delta E)$ is the probability density function for the i th event, q_i denotes the candidate's flavor (charge) ($q_i = +1$ for B^+ and $q_i = -1$ for B^-), and the yield asymmetry is defined as

$$\mathcal{A}_{raw} = \frac{N_{B^-} - N_{B^+}}{N_{B^-} + N_{B^+}}, \quad (3)$$

where $N_{B^+(B^-)}$ is the yield of $B^+(B^-)$ candidates.

We simultaneously fit for $B^+ \rightarrow K^+\pi^0$ and $\pi^\pm\pi^0$ yields, which feed-across to each other, to determine the branching fractions and CP -violating asymmetries. The fraction of signal and feed-across candidates are constrained with Gaussians according to the mean values and statistical uncertainties of corrected ratios ($\varepsilon_{MC}/\varepsilon_{Data}$), which are about 96%, where ε_{MC} and ε_{Data} are PID efficiencies or fake rates in simulation and data, respectively.

To deal with the simulation-data discrepancies in PDF modeling, we fix the shapes of the signals and feed-across, but float their mean shifts and width ratios in M_{bc} and ΔE . The range is constrained to be a Gaussian, whose mean and width is determined from the mean shift and the multiplicative scale-factor in the control sample study. For the $B\bar{B}$ background, we fix the shape and shift the model in ΔE with the mean shift that we obtained from the control sample study. For the $q\bar{q}$ background, we float the shape parameters.

8. MEASUREMENTS OF BRANCHING FRACTIONS AND CP ASYMMETRY

The M_{bc} - ΔE distributions of $B^+ \rightarrow h^+\pi^0$ data are shown in Figure 4, with the fit curve overlaid. Figures 5, 6 show the fits on charge-specific events overlaid on the projection of the $(M_{bc}, \Delta E)$ dimensions. The details of fit results are given below.

1. Branching fractions

The branching fractions are determined as

$$\mathcal{B}_{B^\pm \rightarrow h^\pm \pi^0} = \frac{N_{B^+ \rightarrow h^+\pi^0}}{\epsilon_{h^+\pi^0} \times \mathcal{R}_{PID}^+ \times (1 - \mathcal{A}_{raw}) \times N_{B\bar{B}}} + \frac{N_{B^- \rightarrow h^-\pi^0}}{\epsilon_{h^-\pi^0} \times \mathcal{R}_{PID}^- \times (1 + \mathcal{A}_{raw}) \times N_{B\bar{B}}}. \quad (4)$$

Here $\epsilon_{h^\pm\pi^0}$ is the efficiency for selecting and reconstructing signal as determined from simulation, \mathcal{R}_{PID}^\pm is the ratio of PID selection efficiencies in data and simulation for positive and negative charged particles, $N_{B^\pm \rightarrow h^\pm \pi^0}$ is the number of generated events corresponding

to the data luminosity, and $N_{B\bar{B}}$ is the number of $B\bar{B}$ pairs in the data sample, corresponding to 35.8 million for B^+B^- . We obtain the number of $B\bar{B}$ pairs from the measured integrated luminosity, the $e^+e^- \rightarrow \Upsilon(4S)$ cross section (1.110 ± 0.008) nb [10] (assuming that the $\Upsilon(4S)$ decays exclusively to $B\bar{B}$ pairs), and the $\Upsilon(4S) \rightarrow B^0\bar{B}^0$ branching fraction $f^{00} = 0.487 \pm 0.010 \pm 0.008$ [11]. Table I summarizes the result of fit for branching fractions, signal yields and corrected signal efficiencies ($\epsilon \times \mathcal{R}_{\text{PID}}$).

TABLE I. Fit results for $B^+ \rightarrow h^+\pi^0$ branching fractions. The product $\epsilon \times \mathcal{R}_{\text{PID}}$ is the corrected signal efficiency.

	$B^+ \rightarrow K^+\pi^0$	$B^+ \rightarrow \pi^+\pi^0$
$\mathcal{B} [10^{-6}]$	$11.9^{+1.1}_{-1.0}$	$5.5^{+1.0}_{-0.9}$
Signal yields	$211.0^{+18.8}_{-18.0}$	$83.9^{+14.7}_{-13.9}$
$\epsilon \times \mathcal{R}_{\text{PID}}$	0.247 ± 0.003	0.212 ± 0.002
Mean shift (MeV/ c^2) in M_{bc}		-0.07 ± 0.09
Scale factor in M_{bc}		0.99 ± 0.03
Mean shift (MeV) in ΔE		$-17.63^{+1.35}_{-1.36}$
Scale factor in ΔE		1.11 ± 0.04

2. CP -violating asymmetry

In general, \mathcal{A}_{raw} is due to the combination of genuine CP -violating effects (\mathcal{A}_{CP}) in the decay dynamics and instrumental asymmetries due to differences in interaction or reconstruction probabilities between opposite-charge hadrons. Such a combination is additive for small asymmetries, $\mathcal{A}_{\text{raw}} = \mathcal{A}_{CP} + \mathcal{A}_{det}$, where \mathcal{A}_{det} is the instrumental asymmetry measured by reconstructing the decays $D^+ \rightarrow K_S^0\pi^+$ and $D^0 \rightarrow K^+\pi^-$ to estimate $\mathcal{A}(\pi)$ and $\mathcal{A}(K)$ by $\mathcal{A}(\pi) = \mathcal{A}(K_S^0\pi) - \mathcal{A}(K_S^0)$, $\mathcal{A}(K) = \mathcal{A}(K\pi) - \mathcal{A}(K_S^0\pi) + \mathcal{A}(K_S^0)$. Table II shows the results for instrumental asymmetries. Table III summarizes the results for \mathcal{A}_{CP} , \mathcal{A}_{raw} , signal yields,

TABLE II. Instrumental charge-asymmetries associated with $K^\pm\pi^\mp$, $K_S^0\pi^\pm$, K^\pm , and π^\pm reconstruction, obtained using samples of $D^0 \rightarrow K^-\pi^+$ and $D^+ \rightarrow K_S^0\pi^+$ decays.

Instrumental asymmetry	Value
$\mathcal{A}_{det}(K^+\pi^-)$	-0.010 ± 0.001
$\mathcal{A}_{det}(K_S^0\pi^+)$	$+0.026 \pm 0.019$
$\mathcal{A}_{det}(K^+)$	$+0.017 \pm 0.019$
$\mathcal{A}_{det}(\pi^+)$	$+0.026 \pm 0.019$

and corrected signal efficiencies ($\epsilon \times \mathcal{R}_{\text{PID}}^+$ and $\epsilon \times \mathcal{R}_{\text{PID}}^-$) for B^+ and B^- decays.

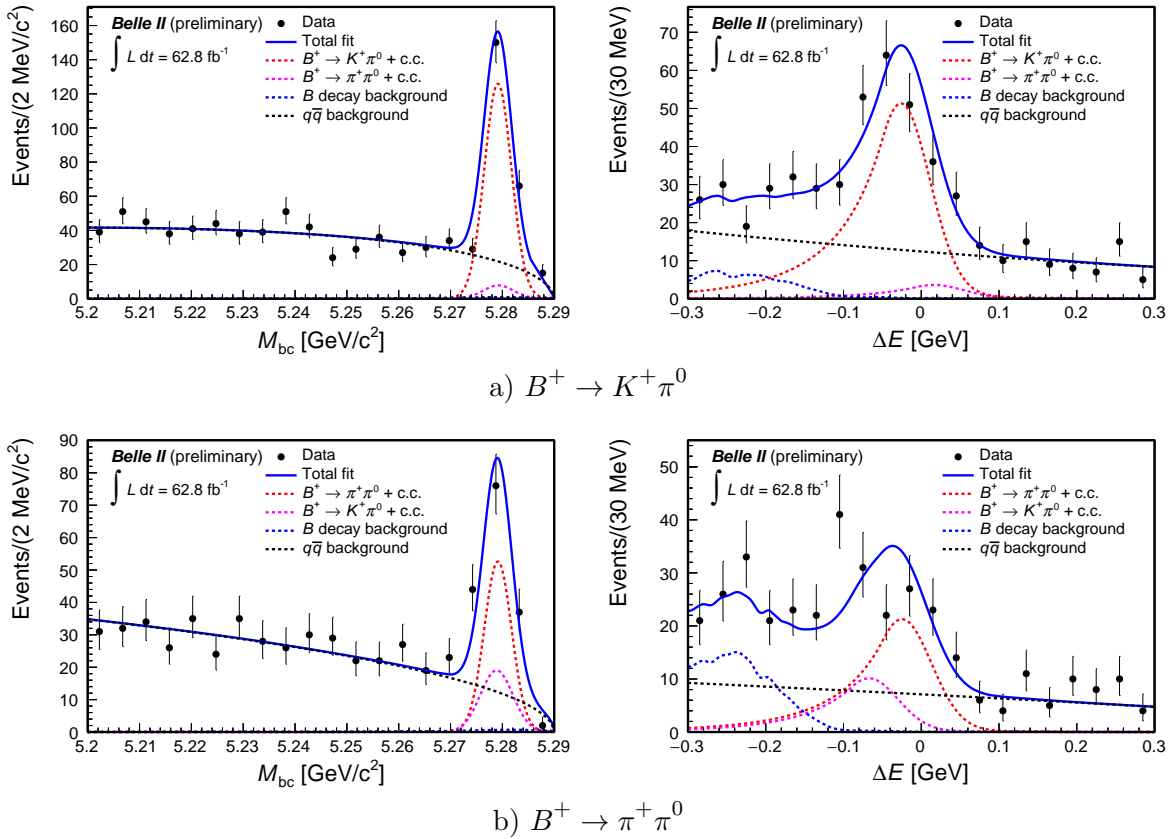


FIG. 4. Distributions of (left) M_{bc} and (right) ΔE for $B^+ \rightarrow h^+ \pi^0$ candidates reconstructed in 2019–2020 Belle II data selected with an optimized continuum-suppression requirement, and projected onto the signal region (left panel: $-0.14 < \Delta E < 0.06$ GeV, right panel: $M_{bc} > 5.27$ GeV/c^2). The projections of the fit are overlaid.

TABLE III. Fit results for $B^+ \rightarrow h^+ \pi^0$ CP -violating asymmetries. The product $\epsilon \times \mathcal{R}_{\text{PID}}^\pm$ is the corrected signal efficiency for positively (negatively) charged h^+ candidates.

	$B^+ \rightarrow K^+ \pi^0$	$B^+ \rightarrow \pi^+ \pi^0$
\mathcal{A}_{CP}	-0.089 ± 0.085	-0.042 ± 0.166
\mathcal{A}_{raw}	-0.072 ± 0.085	-0.016 ± 0.166
B^+ yields	111.1 ± 13.0	42.2 ± 9.8
$\epsilon \times \mathcal{R}_{\text{PID}}^+$	0.243 ± 0.003	0.210 ± 0.002
B^- yields	99.8 ± 12.5	$41.7^{+9.8}_{-9.9}$
$\epsilon \times \mathcal{R}_{\text{PID}}^-$	0.252 ± 0.003	0.214 ± 0.002

9. SYSTEMATIC UNCERTAINTIES

We consider several sources of systematic uncertainties. We assume the sources to be independent, and add in quadrature the corresponding uncertainties. Table IV and V summarize

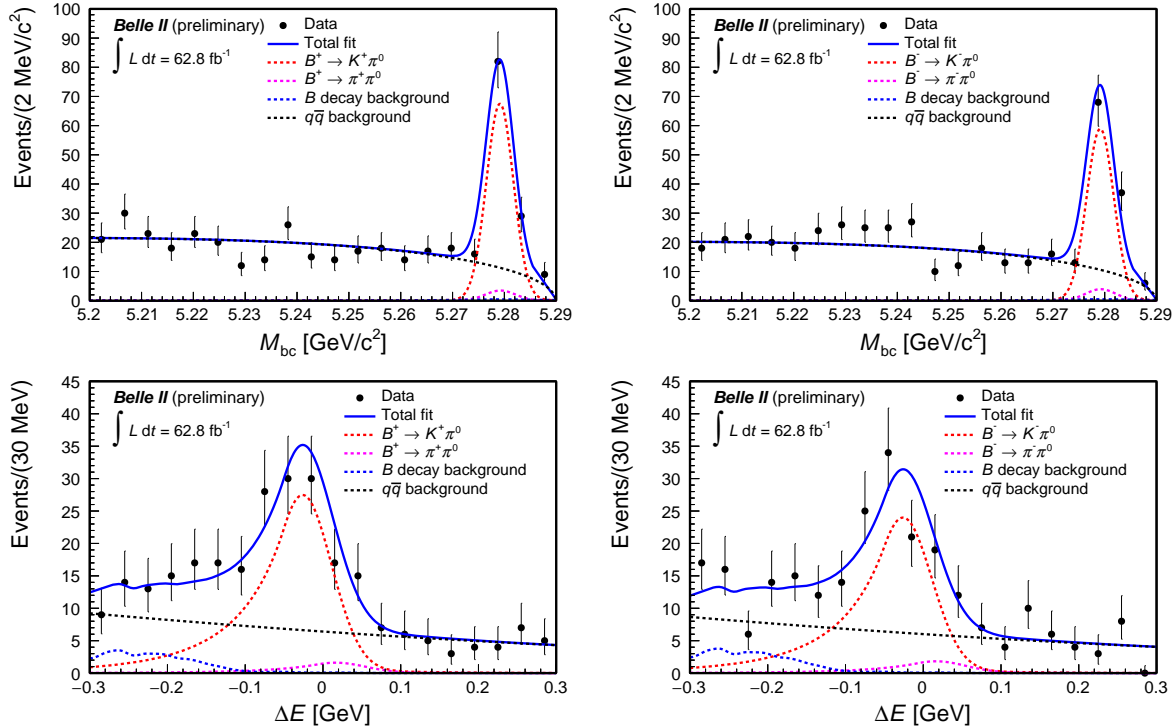


FIG. 5. Charge-specific distributions of (top) M_{bc} and (bottom) ΔE for (left) $B^+ \rightarrow K^+\pi^0$ and (right) $B^- \rightarrow K^-\pi^0$ candidates reconstructed in 2019–2020 Belle II data selected with an optimized continuum-suppression requirement, and projected onto the signal region (top panel: $-0.14 < \Delta E < 0.06 \text{ GeV}$, bottom panel: $M_{bc} > 5.27 \text{ GeV}/c^2$). The projections of the fit are overlaid.

systematic uncertainties for the measurements of the branching fractions and CP -violating asymmetries, respectively.

The systematic uncertainty due to data-simulation discrepancies in charged-particle reconstruction efficiency [12] is estimated to be 0.91% per track. The systematic uncertainty on π^0 reconstruction is studied using the decays $B^0 \rightarrow D^{*-}(\rightarrow \bar{D}^0(\rightarrow K^+\pi^-)\pi^-)\pi^+$, $B^0 \rightarrow D^{*-}(\rightarrow \bar{D}^0(\rightarrow K^+\pi^-\pi^0)\pi^-)\pi^+$ and the ratio of yields between data and simulation. Because the efficiency ratio is compatible with unity, the statistical uncertainty of the ratio is quoted as the systematic uncertainty. The systematic uncertainties in continuum suppression efficiency are evaluated from data-MC discrepancies in the continuum-suppression efficiency using the control channel $B^+ \rightarrow \bar{D}^0(\rightarrow K^+\pi^-\pi^0)\pi^+$. The selection efficiencies obtained in data and simulation agree well; hence the statistical uncertainties on the ratio of data to MC efficiencies are assigned as systematic uncertainties. The systematic uncertainty on the number of $B\bar{B}$ pairs is 1.4% [13].

The fitting systematic uncertainties are due to PDF mismodeling of each component. The uncertainties for signal, feed-across, and continuum are estimated from the difference between the average of results of the sample-composition fit performed on ensembles of simplified simulated experiments generated with the baseline and alternate models. The systematic uncertainties due to data-MC discrepancies in the $B\bar{B}$ background distributions

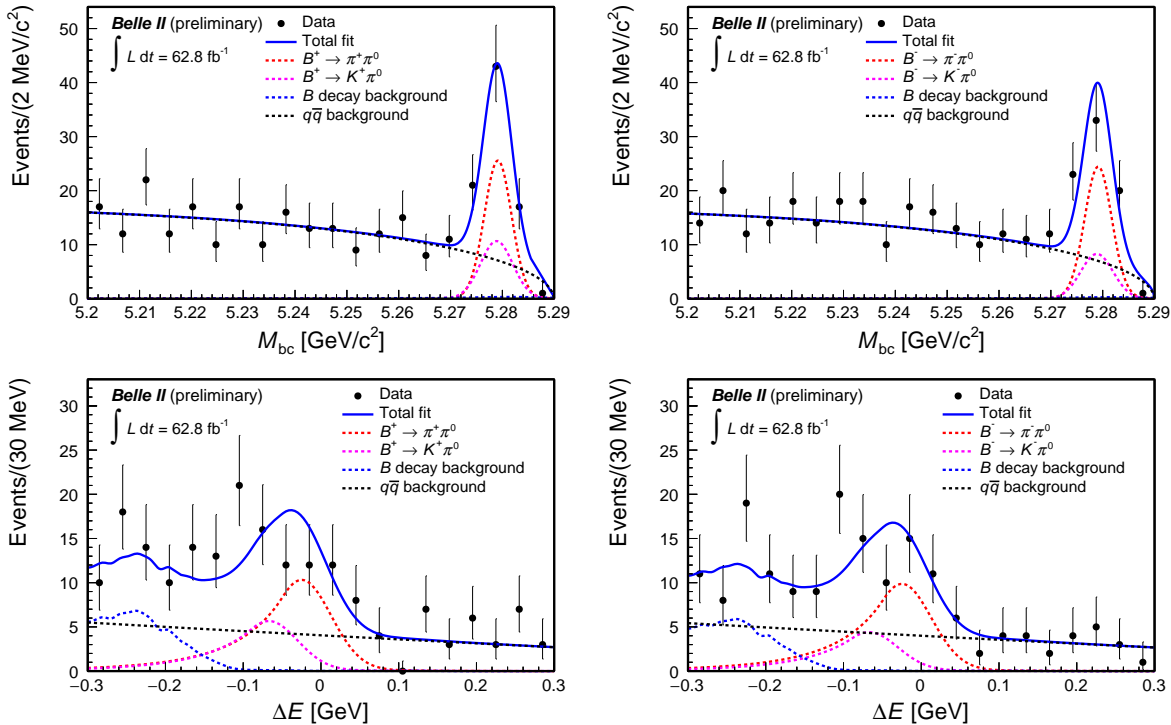


FIG. 6. Charge-specific distributions of (top) M_{bc} and (bottom) ΔE for (left) $B^+ \rightarrow \pi^+\pi^0$ and (right) $B^- \rightarrow \pi^-\pi^0$ candidates reconstructed in 2019–2020 Belle II data selected with an optimized continuum-suppression requirement, and projected onto the signal region (top panel: $-0.14 < \Delta E < 0.06$ GeV, bottom panel: $M_{bc} > 5.27$ GeV/c^2). The projections of the fit are overlaid.

are evaluated by measuring the difference in branching fractions with a more restrictive fitting region, $\Delta E > -0.12$ (GeV).

The systematic uncertainties for the CP -violating asymmetry results due to PDF mismodelling of signal, feed-across, and continuum are estimated from the difference in CP -violating asymmetries while performing fits with an alternative model for each component. The model for each component is assumed to be charge symmetric. We estimate the systematic uncertainties due to model asymmetry by measuring the difference in CP -violating asymmetry with independent charge-specific continuum shape parameters and signal, feed-across mean shifts, and width ratios in M_{bc} and ΔE . The systematic uncertainties due to data-MC discrepancies in the $B\bar{B}$ background distributions are estimated with the same procedure as applied for the branching fractions. A systematic error associated with the uncertainty on the instrumental asymmetry (Table II) is also included.

10. SUMMARY AND CONCLUSION

We report measurements of branching fractions and CP -violating asymmetries of $B^+ \rightarrow h^+\pi^0$ decays using data collected by the Belle II experiment in 2019 and 2020 at the $\Upsilon(4S)$ resonance, corresponding to 62.8 fb^{-1} of integrated luminosity. The branching fractions and direct CP -violating asymmetries are measured to be

$$\mathcal{B}(B^+ \rightarrow K^+\pi^0) = [11.9^{+1.1}_{-1.0}(\text{stat}) \pm 1.6(\text{syst})] \times 10^{-6},$$

TABLE IV. Systematic uncertainties in the branching fraction measurements. The total systematic uncertainty is the sum in quadrature of all the terms.

Source	$B^+ \rightarrow K^+ \pi^0$	$B^+ \rightarrow \pi^+ \pi^0$
Tracking	0.91%	0.91%
π^0 efficiency	13.00%	13.00%
Continuum suppression	2.90%	3.30%
$N_{B\bar{B}}$	1.40%	1.40%
Signal, feed-across model	0.84%	1.37%
$B\bar{B}$ background model	0.40%	1.44%
$q\bar{q}$ background model	0.55%	2.49%
Total	13.47%	13.89%

TABLE V. Systematic uncertainties in the CP -violating asymmetry measurements. The total systematic uncertainty is the sum in quadrature of all the terms.

Source	$B^+ \rightarrow K^+ \pi^0$	$B^+ \rightarrow \pi^+ \pi^0$
Detector bias	0.019	0.019
Signal, feed-across model	0.008	0.004
Background model	0.014	0.059
Total	0.025	0.062

$$\mathcal{B}(B^+ \rightarrow \pi^+ \pi^0) = [5.5^{+1.0}_{-0.9}(\text{stat}) \pm 0.7(\text{syst})] \times 10^{-6},$$

$$\mathcal{A}_{CP}(B^+ \rightarrow K^+ \pi^0) = -0.09 \pm 0.09(\text{stat}) \pm 0.03(\text{syst}), \text{ and}$$

$$\mathcal{A}_{CP}(B^+ \rightarrow \pi^+ \pi^0) = -0.04 \pm 0.17(\text{stat}) \pm 0.06(\text{syst}).$$

The results described above supersede the previous Belle II results reported in Ref [5] using more data and an improved analysis that implements two-dimensional M_{bc} - ΔE fits and a more refined treatment of systematic uncertainties, and are in agreement with world averages [14].

ACKNOWLEDGMENTS

We thank the SuperKEKB group for the excellent operation of the accelerator; the KEK cryogenics group for the efficient operation of the solenoid; and the KEK computer group for on-site computing support. This work was supported by the following funding sources: Science Committee of the Republic of Armenia Grant No. 18T-1C180; Australian Research Council and research grant Nos. DP180102629, DP170102389, DP170102204, DP150103061, FT130100303, and FT130100018; Austrian Federal Ministry of Education, Science and Research, Austrian Science Fund No. P 31361-N36, and Horizon 2020 ERC Starting Grant no. 947006 “InterLeptons”; Natural Sciences and Engineering Research

Council of Canada, Compute Canada and CANARIE; Chinese Academy of Sciences and research grant No. QYZDJ-SSW-SLH011, National Natural Science Foundation of China and research grant Nos. 11521505, 11575017, 11675166, 11761141009, 11705209, and 11975076, LiaoNing Revitalization Talents Program under contract No. XLYC1807135, Shanghai Municipal Science and Technology Committee under contract No. 19ZR1403000, Shanghai Pujiang Program under Grant No. 18PJ1401000, and the CAS Center for Excellence in Particle Physics (CCEPP); the Ministry of Education, Youth and Sports of the Czech Republic under Contract No. LTT17020 and Charles University grants SVV 260448 and GAUK 404316; European Research Council, 7th Framework PIEF-GA-2013-622527, Horizon 2020 Marie Skłodowska-Curie grant agreement No. 700525 ‘NIOBE,’ and Horizon 2020 Marie Skłodowska-Curie RISE project JENNIFER2 grant agreement No. 822070 (European grants); L’Institut National de Physique Nucléaire et de Physique des Particules (IN2P3) du CNRS (France); BMBF, DFG, HGF, MPG, and AvH Foundation (Germany); Department of Atomic Energy under Project Identification No. RTI 4002 and Department of Science and Technology (India); Israel Science Foundation grant No. 2476/17, United States-Israel Binational Science Foundation grant No. 2016113, and Israel Ministry of Science grant No. 3-16543; Istituto Nazionale di Fisica Nucleare and the research grants BELLE2; Japan Society for the Promotion of Science, Grant-in-Aid for Scientific Research grant Nos. 16H03968, 16H03993, 16H06492, 16K05323, 17H01133, 17H05405, 18K03621, 18H03710, 18H05226, 19H00682, 26220706, and 26400255, the National Institute of Informatics, and Science Information NETwork 5 (SINET5), and the Ministry of Education, Culture, Sports, Science, and Technology (MEXT) of Japan; National Research Foundation (NRF) of Korea Grant Nos. 2016R1D1A1B0101035, 2016R1D1A1B02012900, 2018R1A2B3003643, 2018R1A6A1A06024970, 2018R1D1A1B07047294, 2019K1A3A7A09033840, and 2019R1-I1A3A01058933, Radiation Science Research Institute, Foreign Large-size Research Facility Application Supporting project, the Global Science Experimental Data Hub Center of the Korea Institute of Science and Technology Information and KREONET/GLORIAD; Universiti Malaya RU grant, Akademi Sains Malaysia and Ministry of Education Malaysia; Frontiers of Science Program contracts FOINS-296, CB-221329, CB-236394, CB-254409, and CB-180023, and SEP-CINVESTAV research grant 237 (Mexico); the Polish Ministry of Science and Higher Education and the National Science Center; the Ministry of Science and Higher Education of the Russian Federation, Agreement 14.W03.31.0026; University of Tabuk research grants S-0256-1438 and S-0280-1439 (Saudi Arabia); Slovenian Research Agency and research grant Nos. J1-9124 and P1-0135; Agencia Estatal de Investigacion, Spain grant Nos. FPA2014-55613-P and FPA2017-84445-P, and CIDEGENT/2018/020 of Generalitat Valenciana; Ministry of Science and Technology and research grant Nos. MOST106-2112-M-002-005-MY3 and MOST107-2119-M-002-035-MY3, and the Ministry of Education (Taiwan); Thailand Center of Excellence in Physics; TUBITAK ULAKBIM (Turkey); Ministry of Education and Science of Ukraine; the US National Science Foundation and research grant Nos. PHY-1807007 and PHY-1913789, and the US Department of Energy and research grant Nos. DE-AC06-76RLO1830, DE-SC0007983, DE-SC0009824, DE-SC0009973, DE-SC0010073, DE-SC0010118, DE-SC0010504, DE-SC0011784, DE-SC0012704; and the National Foundation for Science and Technology Development (NAFOSTED) of Vietnam under Grant No. 103.99-2020.50.

Appendix A: Non-signal enhanced plots of the fits

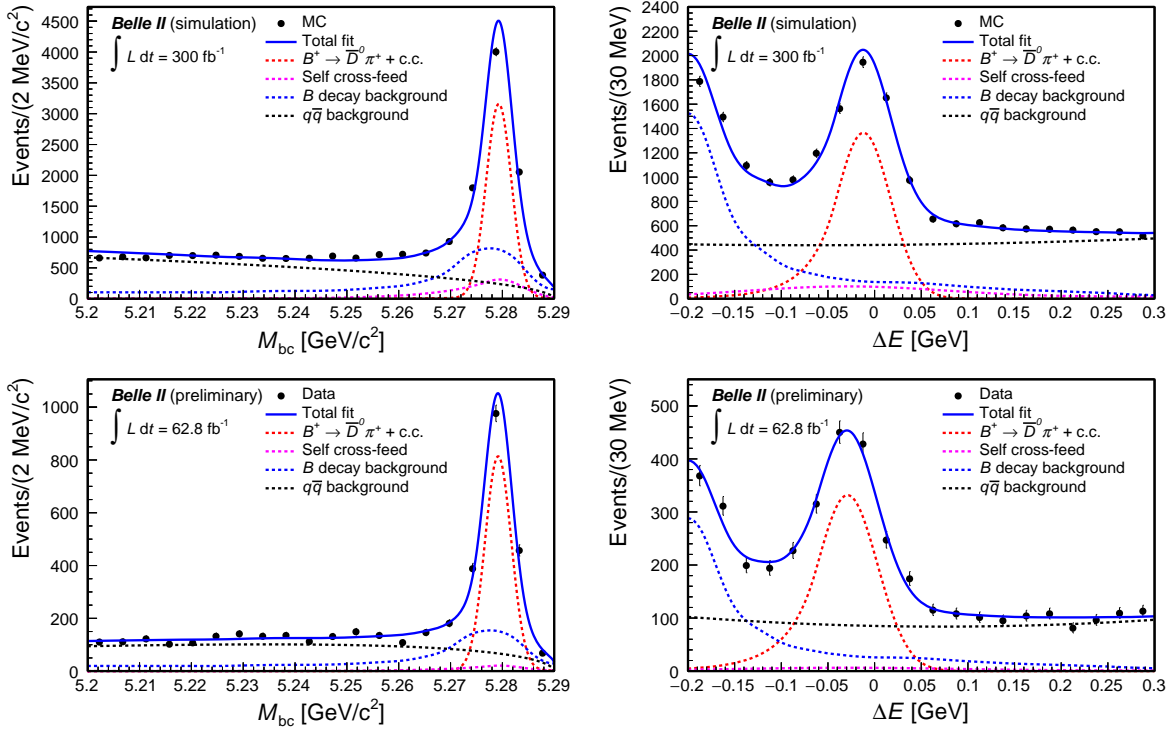


FIG. 7. Distributions of (left) M_{bc} and (right) ΔE for $B^+ \rightarrow \bar{D}^0(\rightarrow K^+\pi^-\pi^0)\pi^+$ candidates reconstructed in (top) simulated events and (bottom) real data selected with an optimized continuum-suppression requirement. The projections of the fit are overlaid.

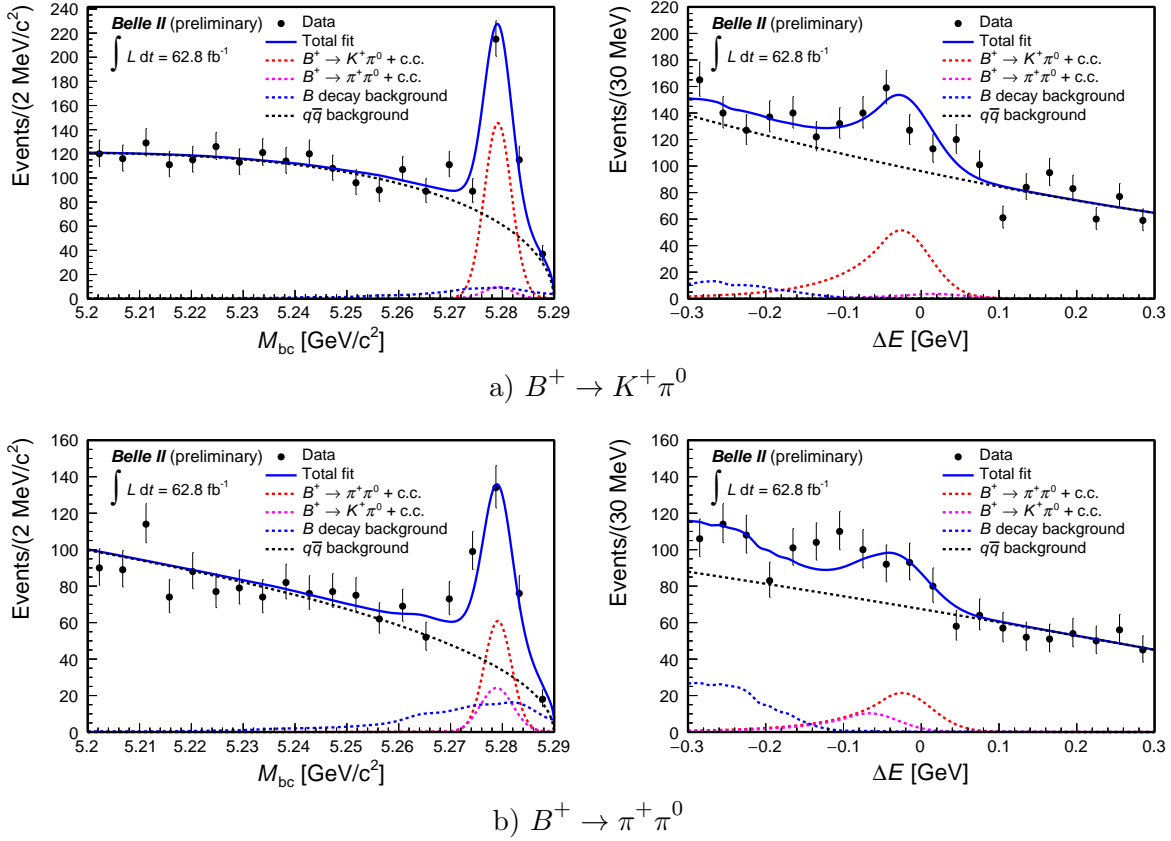


FIG. 8. Distributions of (left) M_{bc} and (right) ΔE for $B^+ \rightarrow h^+ \pi^0$ candidates reconstructed in 2019–2020 Belle II data selected with an optimized continuum-suppression requirement. The projections of the fit are overlaid.

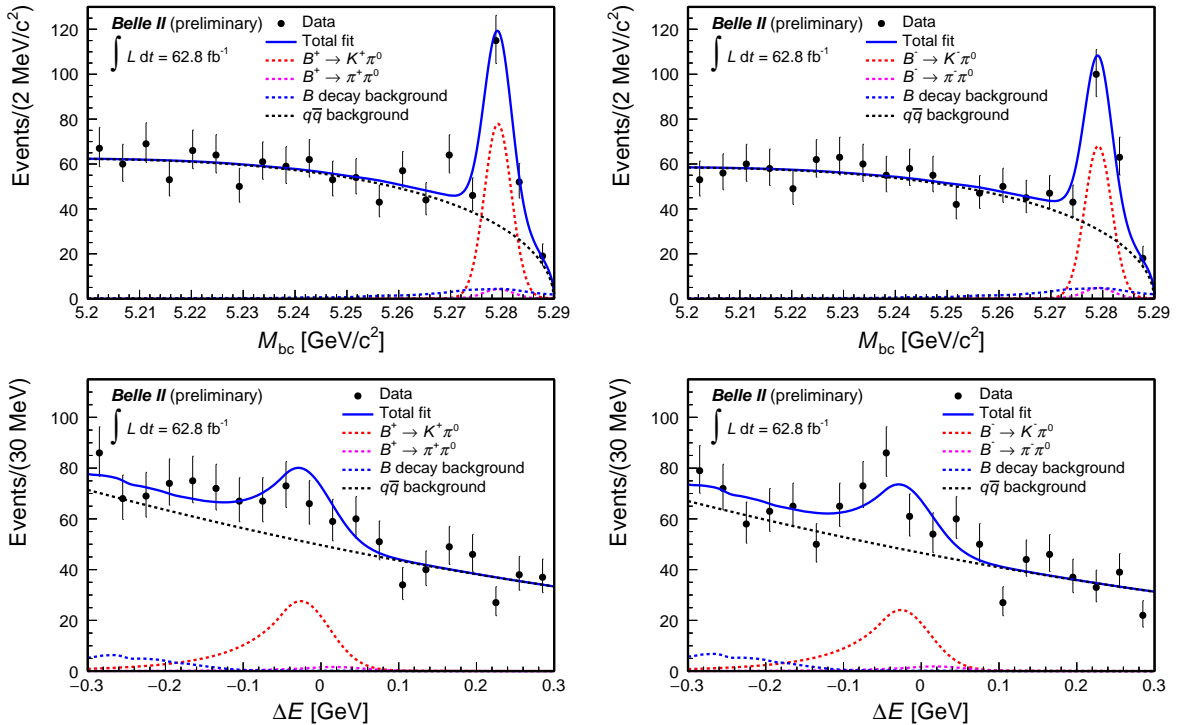


FIG. 9. Charge-specific distributions of (top) M_{bc} and (bottom) ΔE for (left) $B^+ \rightarrow K^+\pi^0$ and (right) $B^- \rightarrow K^-\pi^0$ candidates reconstructed in 2019–2020 Belle II data selected with an optimized continuum-suppression requirement. The projections of the fit are overlaid.

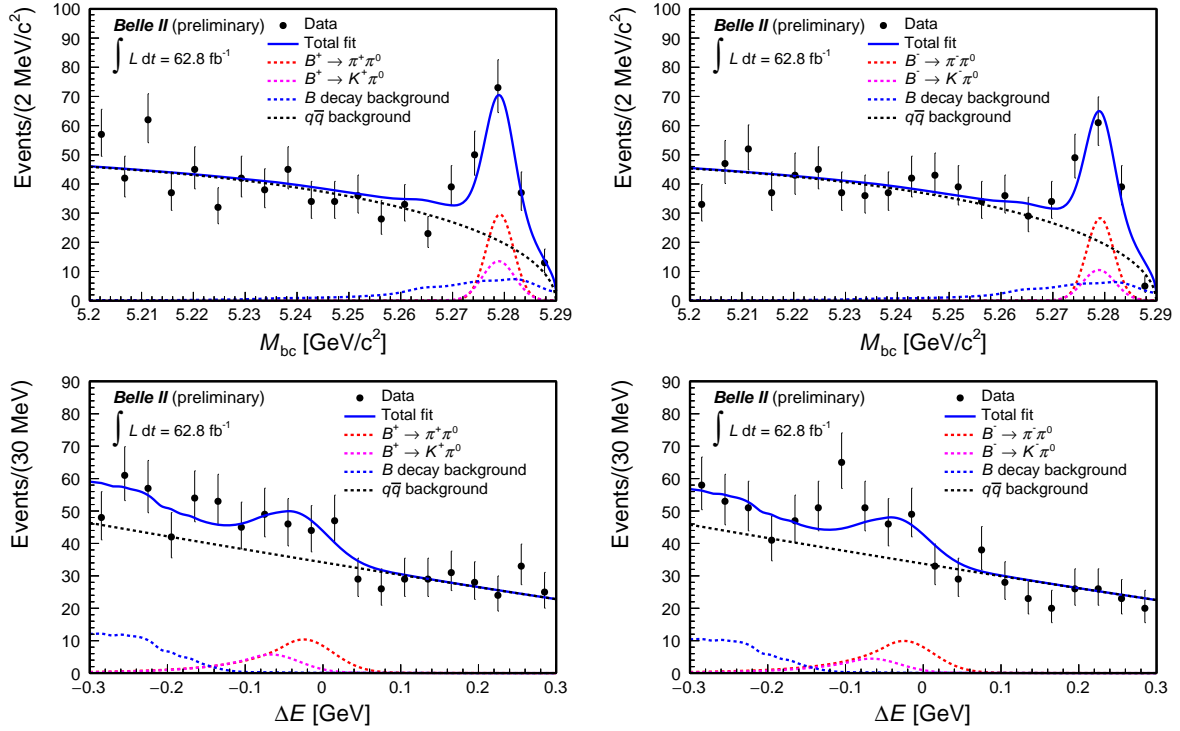


FIG. 10. Charge-specific distributions of (top) M_{bc} and (bottom) ΔE for (left) $B^+ \rightarrow \pi^+\pi^0$ and (right) $B^- \rightarrow \pi^-\pi^0$ candidates reconstructed in 2019–2020 Belle II data selected with an optimized continuum-suppression requirement. The projections of the fit are overlaid.

-
- [1] M. Gronau and J. L. Rosner, Combining CP asymmetries in $B \rightarrow K\pi$ decays, *Phys. Rev. D.* (1999) .
- [2] M. Gronau, A precise sum rule among four $B \rightarrow K\pi$ CP asymmetries, *Phys. Lett. B* **627** (2005) no. 1, 82–88.
- [3] T. Gershon and A. Soni, Null tests of the Standard Model at an International Super B Factory, *J. Phys. G* **34** (2007) 479–492.
- [4] M. Gronau and D. London, Isospin analysis of CP asymmetries in B decays, *Phys. Rev. Lett.* **65** (1990) no. 27, 3381–3384.
- [5] F. Abudinén *et al.* (Belle II Collaboration), Measurements of branching fractions and CP -violating charge asymmetries in charmless B -decay reconstructed in 2019-2020 Belle II data, [arXiv:2009.09452](https://arxiv.org/abs/2009.09452).
- [6] W. Altmannshofer *et al.* (Belle II Collaboration), The Belle II Physics Book, *PTEP* **2019** (2019) no. 12, 123C01.
- [7] T. Abe *et al.* (Belle II Collaboration), Belle II Technical Design Report, [arXiv:1011.0352](https://arxiv.org/abs/1011.0352).
- [8] K. Akai *et al.* (SuperKEKB), SuperKEKB Collider, *Nucl. Instrum. Meth. A* **907** (2018) 188–199.
- [9] T. Kuhr *et al.*, The Belle II Core Software, *Comput. Softw. Big Sci.* **3** (2019) no. 1, 1.
- [10] A. J. Bevan *et al.* (Belle and BaBar Collaborations), The Physics of the B Factories, *Eur. Phys. J. C* **74** (2014) 3026.
- [11] B. Aubert *et al.* (BaBar Collaboration), Measurement of the branching fraction of $\Upsilon(4S) \rightarrow B^0 \bar{B}^0$, *Phys. Rev. Lett.* **95** (2005) 042001.
- [12] V. Bertacchi *et al.*, Belle-II, Track Finding at Belle II, [arXiv:2003.12466](https://arxiv.org/abs/2003.12466).
- [13] F. Abudinén *et al.* (Belle II Collaboration), Measurement of the integrated luminosity of the Phase 2 data of the Belle II experiment, *Chin. Phys. C* **44** (2020) no. 2, 021001.
- [14] P. Zyla *et al.* (Particle Data Group), Review of Particle Physics, to be published in *Prog. Theor. Exp. Phys.* 2020, 083C01 (2020).